Malaysian Journal of Analytical Sciences (MJAS)
Published by Malaysian Analytical Sciences Society

IMMOBILISED Ag-TiO_2/ENR/PVC USING REVERSED PHOTODEPOSITION METHOD FOR PHOTOCATALYTIC DEGRADATION OF METHYLENE BLUE DYE

(Ag-TiO_2/ENR/PVC yang Dipegunkan dengan Menggunakan Kaedah Foto Pendepositan Terbalik untuk Degradasi Foto Pemangkinan Pewarna Metilena Biru)

Nur Izzati Nabilah Zanal, Nureel Imanina Abdul Ghani, Siti Raihan Hamzah, Nur Hafikah Mustapha, Ommy Madina Abdul Halim, NurulFatihah Nazua, Nurul Izzah Roslan, Zuliahani Ahmad, Mohd Fauzi Abdullah, and Wan Izhan Nawawi Wan Ismail*

Faculty of Applied Sciences, Universiti Teknologi MARA (UiTM), 02600 Arau, Perlis, Malaysia

**Corresponding author: wi_nawawi@uitm.edu.my*

Received: 2 April 2024; Accepted: 16 September 2024; Published: 27 October 2024

Abstract

In this study, a reversed photodeposition method was developed to minimise the use of noble metals (NM) as doping agents for photocatalytic enhancement, addressing the high cost associated with commercialisation. Unlike the conventional approach where NM is doped onto titanium dioxide (TiO_2) before immobilisation, this method involves doping NM on the surface of immobilised TiO_2. The immobilisation was achieved through a dip-coating method using a coating solution containing Degussa P-25 TiO_2, epoxidised natural rubber (ENR-50) and polyvinyl chloride (PVC) as the polymer binder. This study focused on doping silver (Ag) on TiO_2/ENR/PVC to form ATEP plates. Doping was carried out at different concentrations (100-500 ppm) using both reversed (R) and normal (N) approaches, with photodeposition times ranging from 1 to 6 hours. The photocatalytic performance of the immobilised ATEP(R) and ATEP(N) was determined through the photodegradation of 12 mg L^{-1} methylene blue (MB) dye. X-ray diffraction (XRD) analysis revealed that the etching of ENR/PVC in the reversed method exposed more TiO_2 crystals. Field emission scanning electron microscopy (FESEM) images also proved that the polymer etching resulted in a more porous TiO_2 structure in the reversed method. Energy-dispersive X-ray spectroscopy (EDX) confirmed that the reversed method achieved a higher weight percentage of Ag, which enhanced the surface plasmonic resonance (SPR) effect and improved photocatalytic performance. The optimal sample, 300-ATEP(R 5h), exhibited a higher rate constant ($k = 0.0495$ min^{-1}) than the 400-ATEP(N) ($k = 0.0463$ min^{-1}) sample over 60 minutes of MB dye degradation. This was due to the more porous TiO_2 structure and the stronger SPR effect of Ag in the reversed sample. The Ag concentration was effectively reduced by half while achieving greater photocatalytic performance in 300-ATEP(R 5h) than in 400-ATEP(N). The photocatalytic performance of the samples produced using the reversed method surpassed that of the normal method, with the optimal sample maintaining stability over six cycles.

Keywords: immobilised TiO_2, photocatalytic degradation, porosity, reversed photodeposition, silver

Abstrak

Dalam kajian ini, kaedah foto pendepositan terbalik telah dibangunkan untuk meminimumkan penggunaan logam berharga (NM) sebagai agen pengedopan untuk penambahbaikan foto pemangkinan supaya menangani kos pengkormesialan yang tinggi. Berlawanan dengan kaedah konvensional yang mengedop NM pada permukaan titanium dioksida (TiO_2) yang belum dipegunkan, kaedah ini melibatkan pengedopan NM pada permukaan TiO_2 yang telah dipegunkan. Pemegunan TiO_2 dicapai melalui kaedah

salutan celup dengan menggunakan larutan salutan yang mengandungi Degussa P-25 TiO_2, getah asli yang diepoksidkan (ENR-50) dan polivinil klorida (PVC) sebagai pengikat polimer. Kajian ini memfokuskan pada pengedopan perak (Ag) pada TiO_2/ENR/PVC untuk membentuk plat ATEP. Pengedopan dilakukan pada pelbagai kepekatan (100-500 ppm) dengan menggunakan kedua-dua kaedah terbalik (R) dan normal (N), dengan masa fotodeposit antara 1 hingga 6 jam. Prestasi foto pemangkinan ATEP(R) dan ATEP(N) yang dipegunkan ditentukan melalui fotodegradasi 12 mg L^{-1} pewarna metilena biru (MB). Analisis pembelauan sinar-X (XRD) menunjukkan bahawa punaran ENR/PVC dalam kaedah terbalik mendedahkan lebih banyak kristal TiO_2. Imej mikroskop electron pengimbasan pancaran medan (FESEM) juga membuktikan bahawa punaran polimer menghasilkan struktur TiO_2 yang lebih berliang dalam kaedah terbalik. Spektroskopi sinar-X pancaran tenaga (EDX) mengesahkan bahawa kaedah terbalik mencapai peratusan berat Ag yang lebih tinggi, yang meningkatkan kesan resonans plasmonik permukaan (SPR) dan prestasi foto pemangkinan. Sampel optimal, 300-ATEP(R 5h), menunjukkan kadar pemalar yang lebih tinggi (k = 0.0495 min^{-1}) berbanding dengan sampel 400-ATEP(N) (k = 0.0463 min^{-1}) sepanjang 60 minit degradasi pewarna MB. Ini disebabkan oleh struktur TiO_2 yang lebih berliang dan kesan SPR Ag yang lebih kuat dalam sampel terbalik. Kepekatan Ag dapat dikurangkan dengan berkesan sebanyak separuh sementara mencapai prestasi foto pemangkinan yang lebih besar dalam 300-ATEP(R 5h) berbanding dengan 400-ATEP(N). Prestasi foto pemangkinan sampel yang dihasilkan dengan menggunakan kaedah terbalik melepasi sampel yang dihasilkan dengan menggunakan kaedah normal, dengan sampel optimum mengekalkan kestabilan selama enam kitaran.

Kata kunci: TiO_2 dipegunkan, degradasi foto pemangkinan, porositi, foto deposit terbalik, perak

Introduction

Textiles and clothing manufacturing significantly impact environmental pollution, global climate change and water scarcity [1]. The textile industry consumes nearly 1.3 trillion gallons of water annually to dye garments, equivalent to filling 2.0 million Olympic-sized swimming pools [2]. Most of this wastewater contains harmful chemicals and dyes that flow untreated into rivers. Several methods, such as physical, biological and chemical treatments, including advanced oxidation processes (AOPs), are used to treat dye wastewater [3]. Photocatalysis is one of the promising techniques under AOPs that shows strong potential for the effective removal of dye pollutants in wastewater [4]. This process involves semiconductors and the production of hydroxyl radicals as the main oxidants to oxidise model pollutants [5].

Titanium dioxide (TiO_2) is a good semiconductor due to its non-toxicity, stability, availability, photochemical activity and low cost [6]. It has the potential to degrade organic pollutants present at or near its surface, achieving complete degradation into H_2O and CO_2. Nevertheless, TiO_2 has a short lifetime of photogenerated electrons and holes, causing them to recombine quickly, thus minimising photocatalytic performance [7]. Besides, its broad bandgap energy of 3.2 eV is only active under ultraviolet (UV) irradiations, which accounts for just 5% of the solar spectrum compared to 45% of visible light [8-9]. Therefore, shifting the TiO_2 absorption spectrum towards the visible region is necessary to fully harness sunlight as an inexpensive and renewable energy source.

Doping TiO_2 with noble metals is a promising approach to achieving a visible light-active photocatalyst and solving the issue of fast electron-hole pair recombination [10]. The first publication on doping TiO_2 with noble metals was reported in 1978 by Tauster et al. [11]. Incorporating noble metals into TiO_2 surfaces increases photocatalytic activity by acting as an electron trap due to the surface plasmonic resonance (SPR) effect between TiO_2-metal junctions, promoting interfacial charge transfer and delaying electron-hole pair recombination [12]. Recently, researchers have preferred using TiO_2 in suspension mode due to its high surface area to surfactant ratio [13-15]. Nevertheless, this practice requires a post-treatment filtration step to separate the nano-sized TiO_2 from the treated wastewater. This separation process is crucial to avoid the loss of catalyst particles and the introduction of new TiO_2 pollutants into the treated water.

The post-separation step, which is expensive, can be overcome by immobilising the TiO_2, allowing it to be recycled and continuously used. Several techniques exist to immobilise TiO_2 onto a solid substrate, such as spray coating [16-17], dip coating from suspension [18-19], sol-gel methods [20-21], sputtering [22-23] and electrophoretic deposition [24-25]. In addition, some researchers have used polymers as binders to immobilise

TiO_2 onto support material. Adding polymers improves adhesiveness, temperature resistance, durability and absorbance affinity towards pollutants [26-27]. Various polymers have been used, including polyvinyl pyrrolidine (PVP) [28], polyethylene glycol (PEG) [18], parylene, polyaniline (PANI) [29], polyethylene terephthalate (PET) [30], fluoropolymer resins, epoxidised natural rubber (ENR) [31], poly(methyl methacrylate) (PMMA), polythiophene, polyvinyl chloride (PVC) [32], polycarbonate (PC), poly(1-napthylamine) (PNA) [33], polycarbazole (PCz) [34] and poly(ethylene dioxy thiophene) (PEDOT)[35].

Polymer binders such as ENR-50 and PVC are commonly used to immobilise TiO_2 due to their adhesiveness and durability. Three grades of ENR are used in the industry based on the degree of epoxidation on its chain structure, namely ENR-10, ENR-25 and ENR-50 [36]. Among them, ENR-50 is the most widely used due to its high polarity [37], high tensile properties and hydrophilicity [38]. PVC is a durable, inexpensive and recyclable thermoplastic polymer. However, PVC is brittle and rigid and has limited thermal stability. Blending PVC with elastomers such as ENR can solve these problems [39].

In this study, silver (Ag) was used as a metal dopant to enhance the photocatalytic performance of TiO_2. However, the high costs associated with noble metals, especially for large-scale production, necessitate a cost-effective approach. Thus, this paper presents a novel reversed photodeposition method with various photodeposition times to minimise the use of noble metals and reduce operating expenses. In this approach, the noble metal is primarily introduced as a dopant on the surface of immobilised TiO_2, contrasting with the conventional method of applying photodeposition on TiO_2 to produce noble metal-doped TiO_2 before immobilisation. To evaluate the performance of the fabricated immobilised Ag-TiO_2/ENR/PVC (ATEP) photocatalyst plate, methylene blue (MB) with the molecular formula of $C_{16}H_{18}N_3SCl$ was used as a model pollutant.

Materials and Methods

Chemicals and materials

The TiO_2 photocatalyst (Degussa P25) nano powder, comprising approximately 80% anatase and 20% rutile, was purchased from Acros Organics, Belgium. The ENR-50 (50% epoxidation) was obtained from Kumpulan Guthrie Sdn. Bhd., Malaysia, and the PVC powder was sourced from Petrochemicals (M) Sdn. Bhd., Malaysia. The toluene (C_7H_8), cetyltrimethylammonium bromide (CTAB) and dichloromethane (DCM; CH_2Cl_2; 99.5%) were purchased from R&M Chemicals, Malaysia. The silver nitrate ($AgNO_3$) and isopropyl alcohol (IPA) were purchased from EvergreenEngineering and Resources, Malaysia. The model pollutant, MB (λ_{max}: 661 nm), was purchased from Sigma-Aldrich (M) Sdn. Bhd., Malaysia. Laboratory-distilled water was used throughout the experiment for preparing all solutions and dilution purposes.

Preparation of ENR-50 solution

To prepare the ENR-50 solution, 24.80 ± 0.05 g of ENR-50 was refluxed in 250 mL of toluene at 88-90 °C until all the ENR-50 was completely dissolved and sticky solution was formed. The prepared ENR solution was then filtered into a screw-cap 250 mL Schott bottle for further use in the preparation of the TiO_2 formulation.

Preparation of PVC solution

To prepare the PVC solution, 4 g of PVC powder was dissolved in 175 mL of DCM solution through sonication using a Crest Ultrasonics model 4NT-1014-6 (50-60 kHz) (New Jersey) for 60 minutes. The homogenised PVC solution was then kept in a screw-cap 250 mL Schott bottle for further use in the preparation of the TiO_2 formulation.

Preparation of TiO_2/ENR/PVC formulation for reversed method

Approximately 20 g of ENR solution and 4 g of PVC solution were mixed using a water bath shaker with horizontal motion at 150 rpm for 4 hours. Then, 20 g of TiO_2 and 0.2273 g of CTAB were slowly added to the ENR/PVC blend under continuous sonication for 12 hours to achieve complete homogenisation of the mixture.

Preparation of immobilised Ag-TiO_2/ENR/PVC formulation for reversed method

The Ag-TiO_2/ENR/PVC composite was immobilised using a simple dip-coating method onto clean glass plates (47 mm x 2 mm, 100 mm thickness). Each glass

plate was initially cleaned in acetone solution and sonicated for 1 minute. The clean glass plates were then dried using an air blower. The homogenised TiO_2 formulation was poured into a coating glass cell. Then, each clean glass plate was dipped into the formulation for 5 seconds (covering up to 3 cm depth) and subsequently pulled up manually at a consistent rate. The dipping process was repeated five times. The coated glass plates were then dried completely using an air blower, and the smooth sides of the coated glass were scrapped off prior to dipping into the Ag solution. The coated glass plates were then dipped into a glass cell containing 50% of 40 mL IPA and 10 mL AgNO3 solution (100, 200, 300, 400 and 500 ppm) in a closed system while being purged with nitrogen (N_2) gas for 30 minutes to prevent oxidation of Ag. The photodeposition was then carried out using a 250-W metal halide lamp (LIKO, Malaysia) for durations of 1.0, 1.5, 2.0, 4.0, 5.0 and 6.0 hours. Finally, the Ag-TiO2/ENR/PVC immobilised plates were completely dried at room temperature and stored in plastic dishes prior to use.

Preparation of Ag-TiO_2 for normal method

The preparation of Ag-TiO_2 was conducted as reported by Bhardwaj et al. with slight modifications [40]. For this procedure, 3 g of TiO_2 was dissolved in a 50% aqueous solution of 40 mL IPA and 10 mL of $AgNO_3$ solution (100, 200, 300, 400 and 500 ppm). The solution was stirred until homogenised. The mixture was then soaked for 5 hours prior to photodeposition. After the soaking period, the mixture was transferred into a Schlenk tube and purged with N_2 gas for 30 minutes to prevent oxidation. The photodeposition process was carried out by irradiating the mixture using a 250-W metal halide lamp (LIKO, Malaysia) for 1 hour under continuous stirring. After the irradiation period, the mixture was filtered using vacuum filtration and washed three times with distilled water. The obtained Ag-TiO_2 was dried at room temperature overnight. The dried sample was then ground and kept in an amber vial for future use.

Preparation of immobilised Ag-TiO_2/ENR/PVC formulation for normal method

The obtained Ag-TiO_2 powder was immobilised using ENR and PVC as the polymer binders to attach the TiO_2 onto the glass support. Approximately 4.0 g of ENR solution and 0.8 g of PVC solution were mixed using a water bath shaker with horizontal motion at 150 rpm for 4 hours. Then, 2 g of Ag-TiO_2 and 0.0227 g of CTAB were slowly added to the ENR/PVC blend under continuous sonication for 12 hours to achieve complete homogenisation of the mixture.

Photocatalytic degradation of MB dye

The experiments using both the normal and reversed methods were conducted with the same reactor to ensure an accurate comparison of the performance of each system. The reactor consisted of a custom-made glass cell containing the photocatalyst plate, a 55-W fluorescent lamp as a visible light source placed horizontally, a reflective sleeve made from aluminium foil to increase reflection, and an aquarium pump for aeration.

For the degradation study, 7 mL of MB dye was poured into the glass cell (L × W × H: 5 x 10 x 8 cm) before placing the immobilised Ag-TiO_2/ENR/PVC glass plate. Before the lamp was switched on to initiate the photocatalytic reaction, the coated glass plate was aerated in dark conditions to achieve complete adsorption/desorption equilibrium with a simultaneous oxygen supply from the NS 7200 model aquarium pump. Then, a 3 mL aliquot of treated MB dye was taken out from the glass cell using a syringe. After measuring the absorbance, the treated dye was dispensed back into the glass cell to maintain the solution volume. Photodegradation took place for 45 minutes, and the absorbance was measured at 15-minute intervals using a UV spectrophotometer (HACH DR1900, United States) at a wavelength of 661 nm.

The degradation rate of MB dye was calculated using the formula in Equation (1),

$$\ln \frac{C}{C_0} = -k_{app} t \qquad (1)$$

where C is the current concentration, C_0 represents the initial concentration and *t* is time. The values were then plotted against irradiation time. The slope of the linear plot was taken as the pseudo-first-order rate constant based on the Langmuir-Hinshelwood rate model [41]. Figure 1 shows the photocatalysis setup for MB degradation.

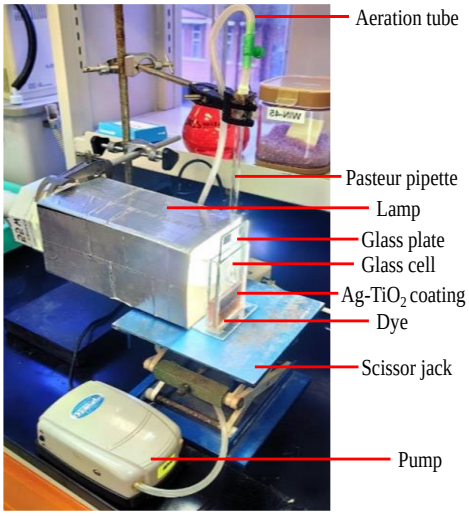

Figure 1. The photocatalysis setup for dye degradation.

Characterisation

Characterisation included several analyses to determine the properties of the Ag-TiO_2/ENR/PVC photocatalyst. Fourier Transform Infrared (FTIR; Perkin Elmer Frontier, USA) with ACD/Spectrus Processor 2020.2.0 software was used to analyse the various functional groups in the photocatalyst within the range of 400-4000 cm^{-1}. The X-ray diffraction (XRD; D5000 Bruker, Germany) with Cu-Kα X-ray energy (1.54 A°) at 45 kV and a diffraction range of 2θ from 20-80° was employed to detect the crystallographic characteristics of the modified Ag-TiO_2/ENR/PVC. Field emission scanning electron microscopy/energy dispersive X-ray spectroscopy (FESEM/EDX) was used to determine the surface morphology and dispersion of the metal on the catalyst surface. The colour changes of the prepared samples were determined by physical observation.

Results and Discussion

Characterisation of ATEP

Degussa P-25 TiO_2 and 100-ATEP(R 5h) to 500-ATEP(R 5h) were subjected to the FTIR analysis. Figure 1 shows the typical IR spectra in the region 4000-600 cm^{-1}. As seen in Figure 2, broad peaks present at 3364 cm^{-1} and 1627 cm^{-1} represent the stretching and bending vibrations of the hydroxyl group (OH) due to water molecules absorbed on the catalyst surface [42]. Water or hydroxyl ions (OH^-) are possible traps for holes (h^+), leading to the formation of hydroxyl radicals (OH•), which are then used to degrade organic compounds [43-44]. The peaks at 1251 cm^{-1} and 1332 cm^{-1} indicate the presence of PVC [45-46], while the peak at 1432 cm^{-1} indicates the presence of the ENR-50 compound [15]. Due to the effect of doping with Ag, the peak for TiO_2 lattice vibration was observed to shift from 1400 cm^{-1} to 1384 cm^{-1}, suggesting the formation of Ag-TiO_2 bonding. Moreover, the two peaks at 2911 cm^{-1} and 2969 cm^{-1} correspond to the alkyl-CH_3 group of the polymer binder [47]. Table 2 exhibits the peaks obtained from the FTIR analysis and their corresponding functional groups.

Figure 3 depicts the XRD patterns for 100-ATEP(R 5h), 300-ATEP(R 5h) and 400-ATEP(N). The figure shows that all samples were investigated in the range of 2θ = 20-80°. According to the JCPDS database, the diffraction peaks were identified as anatase and rutile phases of TiO_2, as this study used commercially available Degussa P-25 TiO_2, which consists of 80% anatase and 20% rutile. The peaks at 2θ = 25.30°, 37.79°, 38.57°, 48.04°, 53.89°, 68.76°, 70.30° and 75.10° were indexed as (101), (103), (004), (200), (105), (116) and (220) and can be assigned as anatase peaks. Meanwhile, rutile peaks at 2θ = 26.95° and 55.07° correspond to Miller indices of (110) and (211), respectively. Commonly, using $AgNO_3$ as the Ag precursor results in the formation of Ag metal (Ag^0) and silver oxide (Ag_2O) in the composite, with Ag_2O being unfavourable for photocatalytic reaction as it can reduce photocatalytic performance [51]. In this study, only the peaks of Ag^0 were observed at 2θ = 44.25° (200), 64.36° (220) and 78.49° (311), while no Ag_2O peak was present [48-50].

Table 1. Experimental conditions and first-order rate constant of ATEP for the degradation of MB dye

Sample	Concentration of $AgNO_3$ (ppm)	1st order rate constant (min^{-1})	
		Reversed (R 5h)	Normal (N)
TiO_2	-	0.0211	0.0106
100-ATEP	100	0.0285	0.0183
200-ATEP	200	0.0338	0.0207
300-ATEP	300	0.0495	0.0303
400-ATEP	400	0.0119	0.0463
500-ATEP	500	0.0098	0.0117

*R 5h refers to the reversed method with 5 hours of photodeposition time

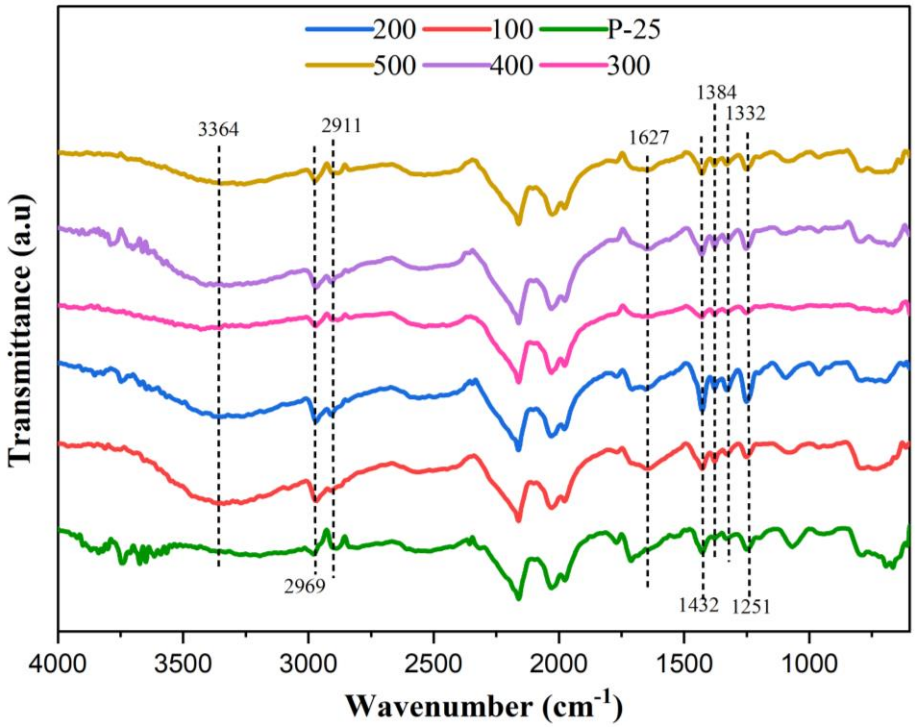

Figure 2. FTIR spectra of Degussa P-25 TiO_2 and 100-ATEP(R 5h) to 500-ATEP(R 5h).

Table 2. FTIR peaks and corresponding functional groups.

FTIR Peak (cm^{-1})	Functional Group Assigned
3364, 1627	Stretching and bending vibration of the hydroxyl group (OH)
1332	CH_2 deformation of PVC
1251	C-H stretching and vibrations of -CHCl groups of PVC
1432	ENR-50
1384	lattice vibration of Ag-TiO_2 (Ti-O-Ag stretching)
2969, 2911	alkyl-CH_3 group

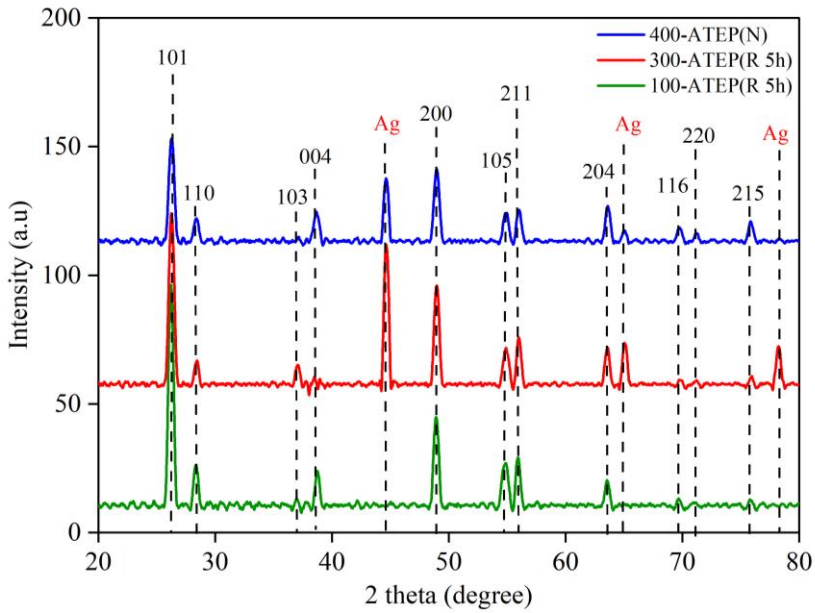

Figure 3. X-ray diffraction patterns of 100-ATEP(R 5h), 300-ATEP(R 5h) and 400-ATEP(N).

Meanwhile, the dominant peak at 2θ = 25.31° (101) corresponds to the TiO_2 anatase phase. The higher peak intensities result from the etching of the polymer, which exposes more TiO_2 crystals to the X-ray probe [32]. This increased exposure facilitated the formation of Ag-TiO_2 as Ag readily combines with the exposed TiO_2 active sites, resulting in an intense Ag peak at 44.25° (200). However, in the 100-ATEP(R 5h) sample, the peak for Ag^0 is not visible even though the intensity peak for (101) is very sharp. This is likely due to the lower concentration of Ag used. The peak intensities of Ag measured at 2θ = 44.25° (200), 64.36° (220) and 78.49° (311) were higher in 300-ATEP(R 5h) than in 400-ATEP(N), showing a two-fold increase in line with the peak at (101). This study found that the reversed method shows better photoetching than the normal method, as observed in the FESEM images. This finding is confirmed by the higher peak intensities of TiO_2 and Ag^0 in the 300-ATEP(R 5h) sample.

Figure 4 depicts the surface morphology and cross-section of 300-ATEP(R 5h) and 400-ATEP(N) after the degradation of MB, as observed using FESEM with EDX. Based on the XRD study, it has been concluded that the reversed method has better photoetching abilities than the normal method. Figure 4(a) displays the surface morphology of 300-ATEP(R 5h), revealing significant aggregation of Ag nanoparticles within a porous TiO_2 framework. After 5 hours of radiation exposure, the polymer binder in the reversed sample underwent etching, resulting in a more porous TiO_2 compared to the normal sample shown in Figure 4(b).

The porous structure of TiO_2 enhances the adsorption of Ag onto the active sites of TiO_2, forming Ag-TiO_2. This process leads to the generation of more radicals ($\bullet O_2^-$ and $\bullet OH$) in the reversed method, hence enhancing its photocatalytic performance. Furthermore, the Ag nanoparticles are evenly dispersed throughout the reversed sample, as seen from the topography resulting from the etching process. The surface morphology of 400-ATEP(N) in Figure 4(b) exhibits a dense surface with minimal porosity, suggesting that the etching process is significantly slower than the reversed method. The surface became smoother as some Ag nanoparticles were hidden below the ENR/PVC layer. This finding is supported by the topography analysis, which shows that the distribution of Ag was irregular. This unequal distribution occurred because the polymer binder covering the Ag nanoparticles was not etched as much, inhibiting Ag from reacting with the TiO_2.

The EDX analysis of the reversed method in Figure 4(a) revealed a decrease in the weight percentage of C (ENR) and Cl (PVC) compared to the normal method shown in Figure 4(b). This observation supports the findings that the leaching of ENR/PVC via the reversed approach was easier and quicker compared to the normal

approach. In addition, the amount of Ag on the surface of the TiO_2 semiconductor was greater at a wt% = 28.3 in the reversed approach, compared to only wt% = 0.1 in the normal approach. The increased reaction between TiO_2 and Ag may be attributed to the leaching effect of the polymer binder ENR/PVC in the reversed approach, leading to greater exposure of TiO_2 active sites for interaction with Ag. Figure 4(c) shows the cross-section of the immobilised 300-ATEP(R 5h) sample. The presence of the Ag-doped TiO_2/ENR/PVC layer is visible, and it is observed that the Ag doping is limited to the top surface of the TiO_2 as predicted. However, the doping layer in Figure 4(d) for 400-ATEP(N) is not easily observable. This could be attributed to the integration of the TiO_2 sample within the ENR/PVC layer, resulting in a highly stable TiO_2/ENR/PVC composite.

Meanwhile, in the normal method, the Ag nanoparticles were evenly dispersed throughout the TiO_2/ENR/PVC layer due to the distribution of Ag across the entire TiO_2 solution during the preparation process. The EDX analysis in Figures 4(c) and 4(d) reveals the existence of sodium (Na), calcium (Ca), magnesium (Mg) and silicon (Si) elements, which are part of the glass substrate employed for immobilising TiO_2. As expected, the weight percentage of Ag in the reversed approach was higher than in the normal approach. The leaching process of the polymer binder in the reversed method is simpler and more effective than the normal method

.

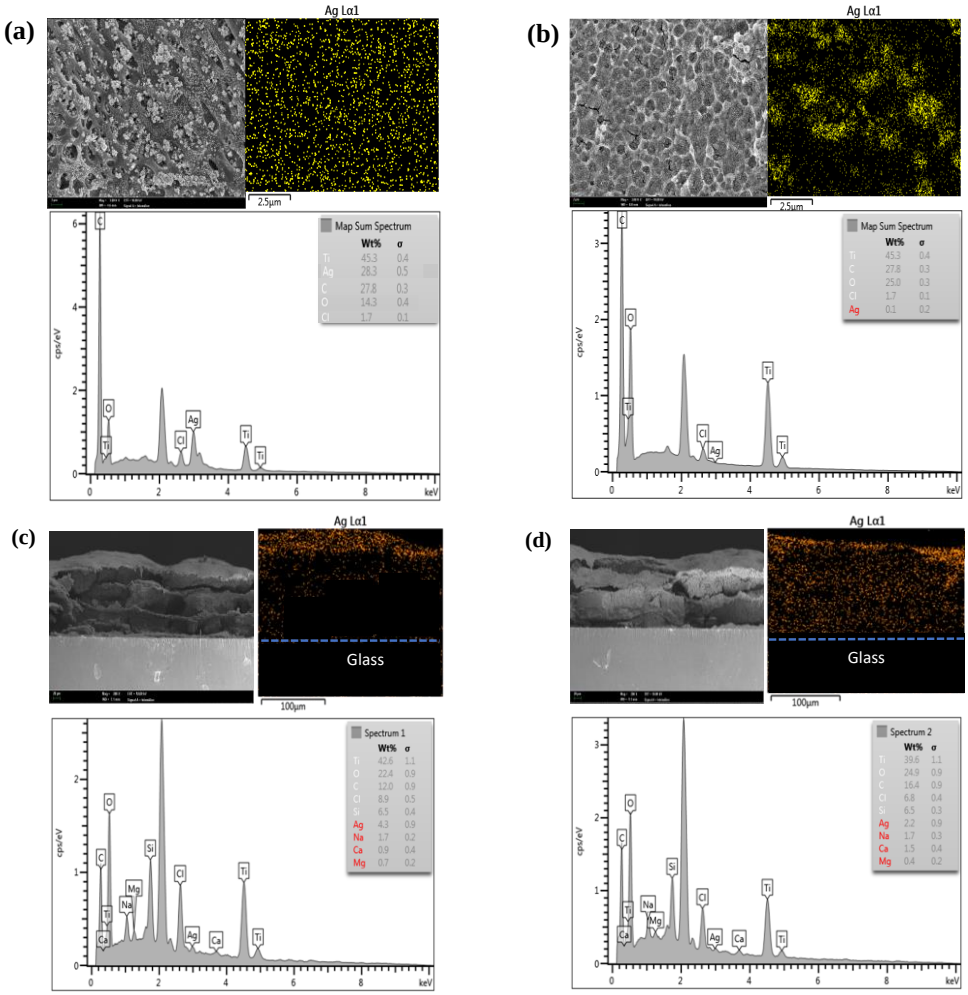

Figure 4. FESEM images of the surface morphology, mapping and EDX for (a) 300-ATEP(R 5h) and (b) 400-ATEP(N); cross-section, mapping and EDX for (c) 300-ATEP(R 5h) and (d) 400-ATEP(N).

Photodegradation of Immobilised Ag-TiO_2/ENR /PVC

The photocatalytic efficiency of the immobilised ATEP for both the reversed and normal methods was evaluated using 12 mg L^{-1} of MB dye as a model pollutant under a 55-W fluorescence lamp. As shown in Figure 5(b), the photocatalytic activity of the immobilised samples produced using the reversed method with 5 hours of photodeposition was one-fold greater than the samples produced using the normal method for all concentrations, except for the 500 ppm sample. For example, the optimal sample, 300-ATEP(R 5h), exhibited a higher k-value than 400-ATEP(N). The immobilised 300-ATEP (R 5h) catalyst plate achieved 96.39% MB degradation within 60 min of light irradiation, whereas the immobilised 400-ATEP(N) catalyst plate decomposed 94.41% of MB, as shown in Figure 5(c).

Figure 5(a) depicts the photocatalytic performance of all samples produced using the reversed method with various photodeposition times. From Figure 5(a), it can be seen that the k-value for unmodified samples (0 ppm) was lower than that of modified samples, except for 500-ATEP. After 1.5 hours of photodeposition, the photocatalytic performance of all samples significantly increased due to the leaching process of ENR/PVC, which exposed more TiO_2 active sites for reaction with Ag and forming Ag-TiO_2. However, the k-value suddenly dropped at the 2-hour mark. This drop is assumed to be due to the continued leaching process during this time, causing the premature formation of Ag-TiO_2, which then leached out together with the binder. Although the leaching of the binder continued after 2 hours of photodeposition, the presence of more $AgNO_3$ (Ag precursor) in the mixture subsequently refilled the active sites of TiO_2, reforming Ag-TiO_2 and increasing the k-value until it reached an optimum at 5 hours. However, for the 400 and 500 ppm samples, the k-value decreased after 1.5 hours because the high concentration of Ag particles on the porous TiO_2 caused more Ag-TiO_2 particles to leach out together with the binder during the leaching process. The photocatalyst performance of the samples produced using the reversed method with a 5-hour optimum photodeposition time was compared with the samples produced using the normal method, as shown in Figure 5(b). All samples produced using the reversed method exhibited a k-value that was one-fold higher than the samples produced using the normal method. The optimal photocatalytic performance was observed in 300-ATEP(R 5h) with a k-value of 0.0495 min^{-1}, while for the normal method, it was 0.0436 min^{-1} in 400-ATEP(N).

The highest photocatalytic performance was observed for 300-ATEP(R 5h), mainly due to the degradation of the organic binder PVC/ENR, which exposed more active sites of TiO_2 for the formation of Ag-TiO_2. This conclusion is supported by XRD and FESEM images. Increasing the concentration of Ag enhances the photocatalytic activity until it reaches an optimal level. However, the 400-ATEP(R 5h) and 500-ATEP(R 5h) samples exhibited a lower rate of photodegradation than the unmodified samples. This occurs as a result of the accumulation and clustering of Ag atoms on the surface of the TiO_2 photocatalyst. An excessive amount of Ag decreases the available surface area for pollutant interactions, specifically with MB dye, thereby reducing the number of active sites for MB and leading to a decrease in photocatalytic efficiency.

Figure 5(d) demonstrates a strong linear correlation ($R^2 > 0.90$) between ln (C_0/C) and irradiation time for unmodified samples, 300-ATEP(R 5h) and 400-ATEP(N). The photocatalytic degradation of MB for all samples adheres to pseudo-first-order kinetics.

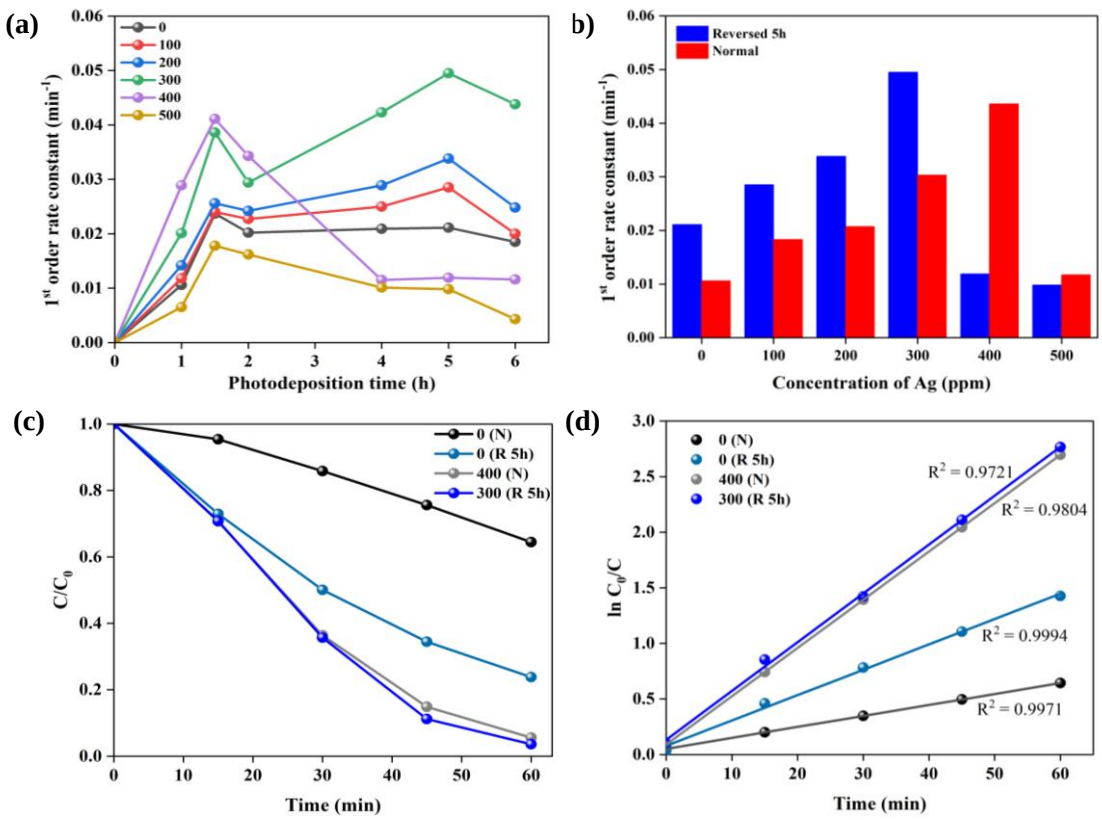

Figure 5. (a) First-order rate constant (k) values of P-25 and ATEP samples produced from the reversed method with various photodeposition times; (b) Comparison of k values for the optimal sample, 300(R 5h), and the sample produced from the normal method; (c) Percentage remaining of MB dye shown as C/C_0; and (d) Plot of ln (C_0/C) versus time.

The objective of immobilising the catalyst onto a solid material is to enable convenient reuse over an extended period. Therefore, an experiment on the reusability and sustainability of the immobilised 300-ATEP(R 5h) catalyst plate was carried out for the degradation of the MB solution. In this study, an immobilised 300-ATEP(R 5h) catalyst plate was repeatedly exposed to a 55-W compact fluorescent lamp for 60 minutes for successive treatments of the MB solution. As observed in Figure 6, the pseudo-first-order rate constant for the first application of the 300-ATEP(R 5h) catalyst plate was the highest, at 0.0459 min^{-1}. After that, the rate constant gradually decreased and stabilised from the fourth to the sixth cycle of application. The calculated average rate constant from the fourth to the sixth cycle was 0.0306 min^{-1}. The percentage decolourisation of the MB solution after one cycle was 95.33%, whereas the percentage removal after the seventh cycle was 51.44%. The decrease in performance by the seventh cycle is due to the peeling off of the catalyst from the glass substrate.

These results indicate that the efficiency of photocatalytic degradation of the MB solution by the immobilised 300-ATEP(R 5h) catalyst remained stable from the first to the sixth cycle. Therefore, the immobilised 300-ATEP(R 5h) catalyst plate showed good reusability and sustainability over extended use. The reduction in the rate constant for the photodegradation of MB dye after the first cycle may result from the adsorption and accumulation of MB substrate or MB intermediates upon irradiation on the catalyst surface [51]. The accumulation of MB molecules could create several layers, obstructing the passage of light to the catalytic surface and decreasing the photodegradation efficiency of the dyes.

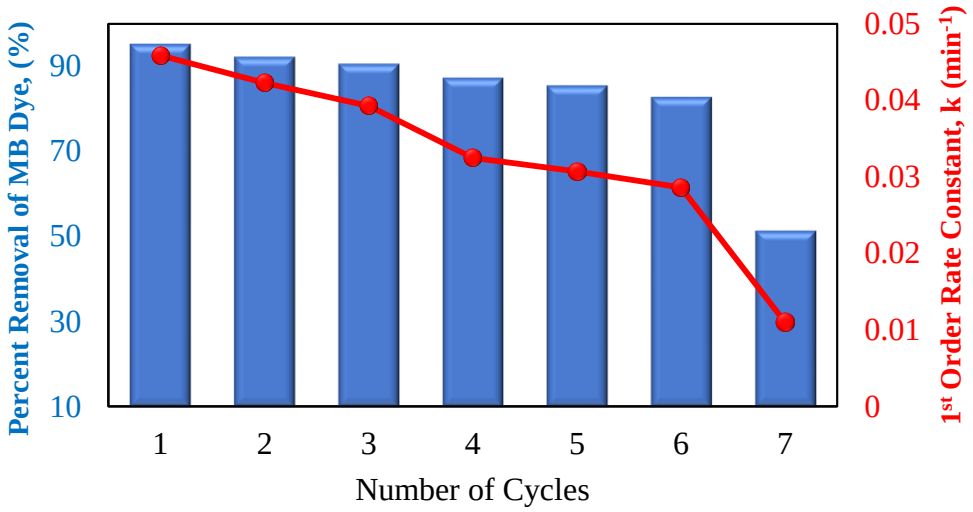

Figure 6. Percentage removal of MB dye (%) and pseudo-first-order rate constant (min^{-1}) vs. number of photocatalysis cycles using the 300-ATEP(R 5h) sample.

Proposed mechanism of modified TiO_2

The photocatalytic mechanism pathway of the immobilised ATEP plate for the photodegradation of MB dye under visible light illumination is illustrated in Figure 7. The reaction is initiated when the semiconductor is exposed to light irradiation with energy greater or equal to the band gap energy of TiO_2. Figure 7(a) depicts the mechanism pathway for the reversed method. After 5 hours of illumination, the porous immobilised TiO_2 is generated due to the leaching of ENR and PVC from the immobilised plate during the photoetching process, as confirmed by the FESEM images. The exposed TiO_2 crystals result in more Ag combining with TiO_2 active sites. The increase in the formation of Ag-TiO_2 leads to more radical formation, which degrades the MB dye.

Upon illumination, electrons in the valence band (VB) move to the conduction band (CB), creating holes (h^+) in the VB and electrons (e^-) in the CB. The photogenerated electrons and holes (e^-/h^+) play an important role in the photodegradation process. Then, the generated e^- interacts with the surrounding oxygen to produce superoxide radicals (•O_2), while h^+ in VB interacts with water to produce hydroxyl radicals (•OH). These reactive oxygen species (ROS), such as •O_2^- and •OH, degrade MB dye into harmless products like CO_2 and H_2O.

Doping TiO_2 with Ag has been proven to reduce the recombination rate of e^-/h^+ pairs because Ag acts as an electron trap, capturing excited electrons from the CB of the TiO_2 semiconductor [10]. These captured electrons are then transferred to surrounding oxygen, forming •O_2^-, while photogenerated h^+ in the VB react with water molecules, aiding in the production of •OH [52]. These free radicals are effectively used for the degradation of MB dye. Moreover, Ag extends the light absorption to the visible light region due to the SPR effect, thereby improving the photocatalytic efficiency of TiO_2 [53].

Figure 7(b) shows the mechanism pathway for immobilised 400-ATEP prepared using the normal method. As seen from the FESEM images in Figure 4(b), it can be concluded that the layer of ENR/PVC in the samples produced using the normal method is quite resistant to leaching, even after 60 minutes of irradiation. This causes most of the Ag-TiO_2 to remain covered under the ENR/PVC layer, decreasing the exposed area of Ag-TiO_2 for interaction with light. This phenomenon results in less generation of •O_2^- and •OH radicals. Therefore, the photocatalytic performance of the samples produced using the normal method is not as efficient as those produced using the reversed method.

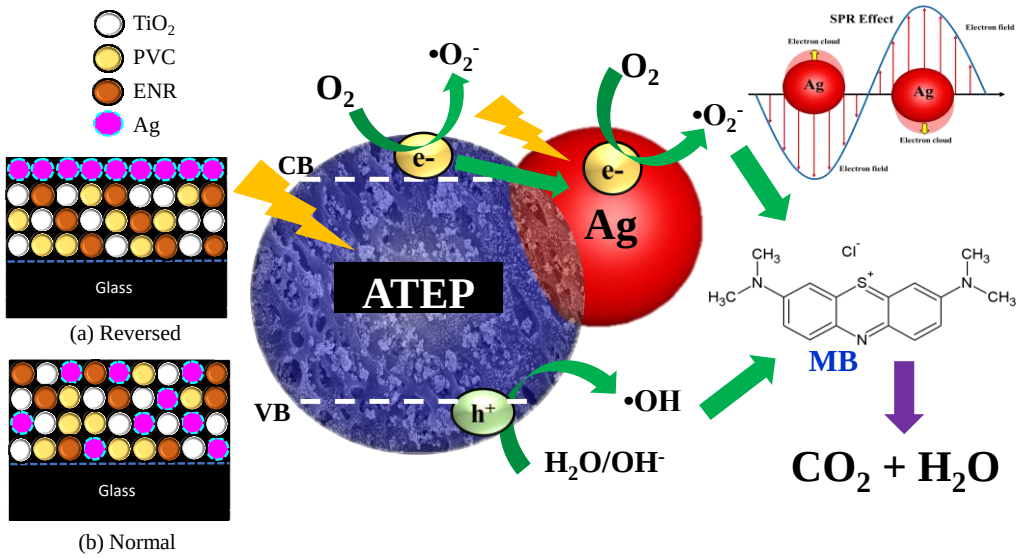

Figure 7. Schematic diagram of immobilised ATEP surface after the photoetching process: (a) sample produced using the reversed method and (b) sample produced using the normal method.

Conclusion

In summary, immobilised ATEP plates were successfully prepared using two different methods: the reversed and the normal methods. Notably, the leaching of the polymer binder ENR/PVC was easier and faster in the reversed method compared to the normal method. This resulted in a more porous TiO_2 structure and promoted the combination of Ag with the active sites, thereby increasing the formation of Ag-TiO_2. The exposure of Ag-TiO_2 to light irradiation generated radicals that effectively degraded MB dye. However, the photocatalytic performance of the samples produced using the normal method was less significant than those produced using the reversed method due to the difficulty in degrading or leaching out the ENR/PVC layer, which covered the formation of Ag-TiO_2 and resulted in fewer radicals. The photocatalytic performance of the 300 ppm Ag-doped sample produced using the reversed method with 5 hours of photodeposition was greater than that of the 400 ppm Ag-doped sample produced using the normal method, with 300-ATEP(R 5h) achieving the highest rate constant at k = 0.0495 min^{-1} and exhibiting stable photocatalytic performance over 6 cycles. Using a less concentrated $AgNO_3$ solution as the Ag precursor in the reversed method yielded better photocatalytic performance than using a more concentrated $AgNO_3$ solution in the normal method. This improvement is attributed to the formation of porous TiO_2, which increases the formation of Ag-TiO_2, the strong SPR effect of Ag and the greater formation of radicals ($•O_2^-$ and •OH) in the reversed method. This study compared two different preparation methods for immobilised Ag-TiO_2, demonstrating that the concentration of Ag can be decreased by one-fold in the reversed method while maintaining excellent photocatalytic performance. These findings offer valuable insights into creating a highly effective photocatalyst for breaking down organic pollutants while minimising costs and time requirements.

Acknowledgement

We would like to express our gratitude to the Ministry of Higher Education, Malaysia, and Universiti Teknologi MARA (UiTM) for their generous internal financial support for this study under the GIP 2023/2 grant: 600-RMC/GIP 5/3 (097/2023), as well as for providing all necessary facilities.

References

1. Boschmeier, E., Ipsmiller, W. and Bartl, A. (2023). Market assessment to improve fibre recycling within the EU textile sector. *Waste Management and Research*, 12: 1-11.
2. Cairns, R. (2023) One-fifth of water pollution comes from textile dyes. Retrieved from https://edition.cnn.com/2023/04/21/middleeast/tex

tile-wastewater-pollutant-cleaner-hnk-scn-spc-intl/index. html.

3. Solayman, H. M., Hossen, M. A., Abd Aziz, A., Yahya, N. Y., Leong, K. H., Sim, L. C., ... and Zoh, K. D. (2023). Performance evaluation of dye wastewater treatment technologies: A review. *Journal of Environmental Chemical Engineering*, 11(3): 109610.
4. Natarajan, S., Bajaj, H. C. and Tayade, R. J. (2018). Recent advances based on the synergetic effect of adsorption for removal of dyes from wastewater using photocatalytic process. *Journal of Environmental Sciences (China)*, 65: 201-222.
5. Nosaka, Y. and Nosaka, A. (2016). Understanding hydroxyl radical (•OH) generation processes in photocatalysis. *ACS Energy Letters*, 1(2): 356-359.
6. Al-Nuaim, M. A., Alwasiti, A. A. and Shnain, Z. Y. (2023). The photocatalytic process in the treatment of polluted water. *Springer Science and Business Media Deutschland GmbH*, 77: 677-701.
7. Koe, W. S., Lee, J. W., Chong, W. C., Pang, Y. L. and Sim, L. C. (2020). An overview of photocatalytic degradation: photocatalysts, mechanisms, and development of photocatalytic membrane. *Environmental Science and Pollution Research*, 27(3): 2522-2565.
8. Etacheri, V., Di Valentin, C., Schneider, J., Bahnemann, D. and Pillai, S. C. (2015). Visible-light activation of TiO_2 photocatalysts: Advances in theory and experiments. *Journal of Photochemistry and Photobiology C: Photochemistry Reviews*, 25: 1-29.
9. Duan, Z., Huang, Y., Zhang, D. and Chen, S. (2019). Electrospinning fabricating Au/TiO_2 network-like nanofibers as visible light activated photocatalyst. *Scientific Report*, 9(1): 1-8.
10. Pathak, T. K., Kroon, R. E., Craciun, V., Popa, M., Chifiriuc, M. C. and Swart, H. C. (2019). Influence of Ag, Au and Pd noble metals doping on structural, optical and antimicrobial properties of zinc oxide and titanium dioxide nanomaterials. *Heliyon*, 5(13): 1333.
11. Tauster, S. J., Fung, S. C. and Garten, R. L. (1978). Strong metal-support interactions. Group 8 noble metals supported on TiO_2.
12. Chakhtouna, H., Benzeid, H., Zari, N., El kacem Qaiss, A. and Bouhfid, R. (2021). Recent progress on Ag/TiO_2 photocatalysts: Photocatalytic and bactericidal behaviors. *Environmental Science and Pollution Research*, 28(33): 44638–44666.
13. Ikhwan, M. S., Nazeri, N. S., Natar, N. S., Abdul Ghani, N. I., Hamzah, S. R., Rosli, M. A., ... and Wan Ismail, W. I. N. (2022). The surface distribution and recyclability study on photodegradation methylene blue dye of immobilized TiO_2 under surfactant effect. *Science Letters*, 16(2): 40-50.
14. Tetteh, E. K., Rathilal, S. and Naidoo, D. B. (2020). Photocatalytic degradation of oily waste and phenol from a local South Africa oil refinery wastewater using response methodology. *Scientific Reports*, 10(1): 8850.
15. Nawi, M. A., and Zain, S. M. (2012). Enhancing the surface properties of the immobilized Degussa P-25 TiO_2 for the efficient photocatalytic removal of methylene blue from aqueous solution. *Applied Surface Science*, 258(16): 6148-6157.
16. Lu, Y., Peng, Y. and Shi, Z. (2023). Plasma sprayed Al_2O_3–40%TiO_2 coating by laser remelting: Structural evolution, tribological properties and DFT calculation, *Tribolology International*, 189: 109009.
17. Hu, H., Mao, L., Xiao, J., Sun, G., Liao, H. and Zhang, C. (2023). Effect of hydrogen flow rate on microstructure and tribological properties of plasma-sprayed Cr_2O_3-65%TiO_2 composite coatings. *Tribolology International*, 189: 108393.
18. Mungsuk, C., Yommee, S., Supothina, S. and Chuaybamroong P. (2023). Solar photocatalytic degradation of carbendazim in water using TiO_2 particle- and sol-gel dip-coating filters. *Results in Engineering*, 19: 101348.
19. Deepa, M. J., Arunima, S. R. and Shibli, S. M. A. (2022). Hydrophobic and corrosion-resistant composite ($BiVO_4$/TiO_2) hot-dip zinc coating with enhanced self-cleaning ability. *Journal of Alloys and Compound*, 924: 166522.
20. Albaidani, K., Timoumi, A., Belhadj, W., Alamri, S. N and Ahmed, S. A. (2023). Structural, electronic and optical characteristics of TiO_2 and Cu-TiO_2 thin films produced by sol-gel spin coating. *Ceramic International*, 49(22): 36265-36275.
21. Pratima B. M. and Subrahmanyam, A. (2022). Protective coatings on copper using as-deposited sol-gel TiO_2-SiO_2 films. *Materials Today Proceedings*, 80: 1061-1065.

22. Villamayor, A., Pomone, T., Perero, S., Ferraris, M., Barrio, V. L., Eva, G., and Kelly, P. (2023). Development of photocatalytic nanostructured TiO_2 and NiO/TiO_2 coatings by DC magnetron sputtering for photocatalytic applications. *Ceramics International*, 49(11): 19309-19317.
23. Regmi G. and Velumani, S. (2023). Radio frequency (RF) sputtered ZrO_2-ZnO-TiO_2 coating: An example of multifunctional benefits for thin film solar cells on the flexible substrate. *Solar Energy*, 249: 301-311.
24. Yun, T. H., Kim, T. Kim, M. T., Park, J. H. and Kim, S. J. (2023). Enhancing corrosion resistance of carbon steel and stainless steel through photocathodic protection using TiO_2-polyvinyl butyral electrophoretic deposition coating. *Journal of Industrial and Engineering Chemistry*, 126: 408-417.
25. Khanmohammadi, S., Ojaghi-Ilkhchi, M .and Farrokhi-Rad M. (2021). Development of bioglass coating reinforced with hydroxyapatite whiskers on TiO_2 nanotubes via electrophoretic deposition. *Ceramic International*, 47(1): 1333-1343.
26. Nawawi, W. I., Zaharudin, R., Ishak, M. A. M., Ismail, K. and Zuliahani, A. (2017). The preparation and characterization of immobilized TiO_2/PEG by using DSAT as a support binder. *Applied Sciences (Switzerland)*, 7(1): 24.
27. Wan Ismail, W. I. N., Ain, S. K., Zaharudin, R., Jawad, A. H., Ishak, M. A. M., Ismail, K., and Sahid, S. (2015). New TiO_2/DSAT Immobilization system for photodegradation of anionic and cationic dyes. *International Journal of Photoenergy*, 2015: 232741.
28. Chandra Pragada S. and Thalla, A. K. (2021). Polymer-based immobilized Fe_2O_3–TiO_2/PVP catalyst preparation method and the degradation of triclosan in treated greywater effluent by solar photocatalysis. *Journal of Environmental Management*, 296: 113305.
29. Riaz, U. and Zia, J. (2020). Microwave-assisted rapid degradation of DDT using nanohybrids of PANI with SnO_2 derived from *Psidium guajava* extract. *Environmental Pollution*, 259: 113917.
30. Ribeiro, L. N., Fonseca, A. C., da Silva, E. F., Oliveira, E. D., Ribeiro, A. T., Maranhão, L. C., ... and Almeida, L. C. (2020). Residue-based TiO_2/PET photocatalytic films for the degradation of textile dyes: A step in the development of green monolith reactors. *Chemical Engineering and Processing - Process Intensification*, 147: 107792.
31. Rosli, M. A., Hamzah, S. R., Muhamad, N. A., Ghani, N. I., Natar, N. S., Ikhwan, S., ... and Ramli, M. Z. (2022). Acid photo etching effect of epoxidized natural rubber (ENR) and polyvinyl chloride (PVC) as polymer binder. *Malaysian Journal of Chemistry*, 24(2): 228-239.
32. Hamzah, S. R., Rosli, M. A., Natar, N. S., Ghani, N. I. A., Muhamad, N. A., Azami, M. S., ... and Nawawi, W. I. (2023). The crosslinking and porosity surface effects of photoetching process on immobilized polymer-based titanium dioxide for the decolorization of anionic dye. *Colorants*, 2(1): 73-89.
33. Zia, J., Farhat, S. M., Aazam, E. S. and Riaz, U. (2021). Highly efficient degradation of metronidazole drug using $CaFe_2O_4$/PNA nanohybrids as metal-organic catalysts under microwave irradiation. *Environmental Science and Pollution Research*, 28(4): 4125-4135.
34. Zia, J., Aazam, E. S. and Riaz, U. (2020). Synthesis of nanohybrids of polycarbazole with α-MnO_2 derived from Brassica oleracea: A comparison of photocatalytic degradation of an antibiotic drug under microwave and UV irradiation. *Environmental Science and Pollution Research*, 271(9): 24173-24189.
35. Munusamy, S., Suresh, R., Giribabu, K., Manigandan, R., Kumar, S. P., Muthamizh, S., ... and Narayanan, V. (2019). Synthesis and characterization of GaN/PEDOT–PPY nanocomposites and its photocatalytic activity and electrochemical detection of mebendazole. *Arabian Journal of Chemistry*, 12(8): 3565-3575.
36. Norfarhana, A. S., Ilyas, R. A., Ngadi, N., Sharma, S., Sayed, M. M., El-Shafay, A. S., and Nordin, A. H. (2022). Natural fiber-reinforced thermoplastic ENR/PVC composites as potential membrane technology in industrial wastewater treatment: A review. *Polymers*, 14(12): 2432.
37. Ahmad Fuad, M. Y., Mohd Ishak, Z. A. and Mohd Omar, A. K. (1995). Determination of filler content in thermoplastic composites by FTIR analysis. *Journal of Applied Polymer Science*, 51: 1875.
38. Yoksan, R. (2008). Epoxidized natural rubber for adhesive applications. *Agricultural and Natural Resources*, 42(5): 325-332.

39. Rachtanapun, P., Kodsangma, A., Homsaard, N., Nadon, S., Jantrawut, P., Ruksiriwanich, W., ... and Jantanasakulwong, K. (2021). Thermoplastic mung bean starch/natural rubber/sericin blends for improved oil resistance. *International Journal of Biomolecule Macromolecule*, 188: 283-289.
40. Bhardwaj, S., Sharma, D., Kumari, P. and Pal, B. (2020). Influence of photodeposition time and loading amount of Ag co-catalyst on growth, distribution and photocatalytic properties of Ag@TiO_2 nanocatalysts. *Optical Materials*, 106: 109975.
41. Karthik, P., Ravichandran, S., Sasikala, V., Prakash, N., Mukkannan, A. and Rajesh, J. (2023). Effective photodegradation of organic water pollutants by the facile synthesis of Ag_2O nanoparticles. *Surfaces and Interfaces*, 40: 103088.
42. Saoud, K., Alsoubaihi, R., Bensalah, N., Bora, T., Bertino, M. and Dutta, J. (2015). Synthesis of supported silver nano-spheres on zinc oxide nanorods for visible light photocatalytic applications. *Materials Research Bulletin*, 63:134-140.
43. Zhang, X., Wang, D., Man, X., Wu, J., Liu, Q., Qi, Y., ... and Hao, C. (2020). Influence of $BiOIO_3$ morphology on the photocatalytic efficiency of Z-scheme $BiOIO_3$/g-C_3N_4 heterojunctioned composite for HgO removal. *Journal Colloid Interface Science*, 558: 123-136.
44. Kunnamareddy, M., Diravidamani, B., Rajendran, R., Singaram, B. and Varadharajan, K. (2018). Synthesis of silver and sulphur codoped TiO_2 nanoparticles for photocatalytic degradation of methylene blue. *Journal of Materials Science: Materials in Electronics*, 29(21): 18111-18119.
45. Nawi, M. A., Ngoh, Y. S. and Zain, S. M. (2012). Photoetching of immobilized TiO_2 - ENR50 -PVC composite for improved photocatalytic activity. *International Journal of Photoenergy*, 2012: 859294.
46. Hamzah, S. R., Rosli, M. A., Natar, N. S., Ghani, N. I. A., Muhamad, N. A., Azami, M. S., ... & Nawawi, W. I. T. (2022). The crosslinking and porosity surface effects of immobilized TiO_2/ENR/PVC via photoetching process for photocatalytic enhancement under photodegradation of RR4 dye. *SSRN Paper*, 2022: 4206591
47. Ramezani, M., Amoozegar, M. A. and Ventosa, A. (2015). Screening and comparative assay of poly-hydroxyalkanoates produced by bacteria isolated from the Gavkhooni Wetland in Iran and evaluation of poly-β-hydroxybutyrate production by halotolerant bacterium Oceanimonas sp. GK1. *Annals of Microbiolology*, 65(1): 517-526.
48. You, X., Chen, F., Zhang, J. and Anpo, M. (2005). A novel deposition precipitation method for preparation of Ag-loaded titanium dioxide. *Catalyst Letters*, 102(3-4): 247-250.
49. Jemal, K., Sandeep, B. V. and Pola, S. (2017). Synthesis, characterization, and evaluation of the antibacterial activity of *Allophylus serratus* leaf and leaf derived callus extracts mediated silver nanoparticles. *Journal of Nanomaterials*, 2017: 4213275.
50. Kumar, S. V., Bafana, A. P., Pawar, P., Rahman, A., Dahoumane, S. A. and Jeffryes, C. S. (2018). High conversion synthesis of <10 nm starch-stabilized silver nanoparticles using microwave technology. *Scientific Reports*, 8(1): 5106.
51. Huang, Q., Liu, S., Wei, W., Yan, Q. and Wu, C. (2015). Selective synthesis of different ZnO/Ag nanocomposites as surface enhanced Raman scattering substrates and highly efficient photocatalytic catalysts. *RSC Advanced*, 5(34): 27075-27081.
52. Din, M. I., Khalid, R. and Hussain, Z. (2018). Minireview: Silver-doped titanium dioxide and silver-doped zinc oxide photocatalysts. *Analytical Letters*, 51(6): 892-907.
53. Furube A. and Hashimoto S. (2017). Insight into plasmonic hot-electron transfer and plasmon molecular drive: new dimensions in energy conversion and nanofabrication. *NPG Asia Materials*, 9(12): 454